Research Article

Efficient Separation of Organic Dyes using Polyvinylidene Fluoride/Polyethylene Glycol-Tin Oxide (PVDF/PEG-SnO_2) Nanoparticles Ultrafiltration Membrane

Abdullah Ghanim Saleem
Department of Chemical Engineering, College of Engineering, University of Baghdad, Baghdad, Iraq
Department of Chemical and Petrochemical Engineering, College of Engineering, University of Anbar, Anbar, Iraq

Sama Mohammed Al-Jubouri*
Department of Chemical Engineering, College of Engineering, University of Baghdad, Baghdad, Iraq

* Corresponding author. E-mail: sama.al-jubouri@coeng.uobaghdad.edu.iq DOI: 10.14416/j.asep.2024.08.001
Received: 16 May 2024; Revised: 29 June 2024; Accepted: 9 July 2024; Published online: 1 August 2024

Abstract
This work studies developing ultrafiltration (UF) membranes using organic and inorganic additives to remove organic dyes at UF conditions with high effectiveness. Flat sheet (18 wt%) polyvinylidene fluoride (PVDF) membranes were prepared via phase inversion and then developed by adding 6 wt% polyethylene glycol (PEG) as a pore former. Furthermore, the PVDF/PEG membranes were developed by embedding tin oxide nanoparticles (SnO_2 NPs) with different contents of 0.3, 0.6, and 0.9 wt%. The prepared membranes were examined for their performance in the dye removal before being characterized using the field emission scanning electron microscope, atomic force microscopy, contact angle, Fourier-transform infrared spectroscopy, surface charge, porosity, mean pore size, tensile strength, and elongation at break. The performance was tested regarding pure water flux (PWF), permeate flux, and dye removal (R%). The effect of dye concentration and pH of the feed solution on the permeate flux and R% was also investigated. In addition, the antifouling features in terms of flux recovery ratio, reversible fouling, irreversible fouling, total fouling, and the R% were studied using the PVDF/PEG membrane and the membrane containing 0.3 wt% of SnO_2 NPs. The contact angle decreased from 78.85° to 51.88°, and the PWF rose from 7.16 to 135.71 L/m^2.h for PVDF and PVDF/PEG-SnO_2 (0.3 wt%) membranes, respectively. The R% of rhodamine B (RhB) slightly decreased from 93.08 to 91.26, and 87.71% for PVDF, PVDF/PEG, and PVDF/PEG-SnO_2 (0.3 wt%) membranes, respectively. Then, it increased with increasing NPs concentration up to 90.17 and 92.23% for PVDF/PEG-SnO_2 (0.6 wt%) and PVDF/PEG-SnO_2 (0.9 wt%) membranes, respectively. Also, the molecular weight cutoff was calculated using RhB as a cationic dye, acid orange 10, and congo red as an anionic dye and it was 520 Da.

Keywords: Anionic dyes, Cationic dyes, Mixed matrix membrane, PEG, PVDF membrane, Tin oxide (SnO_2)

1 Introduction

Water pollution continuously increases due to rapid population growth and industrial development [1], [2]. Although almost three-quarters of the earth is water, the availability of pure water is not easily affordable [3]. Therefore, the scientific community has a great interest in treating polluted water to guarantee safe human health and ecosystems [4]. The industrial waste of chemicals, petroleum, dyes, etc. is the reason for water pollution [5]. Organic dyes are the main source of dye-containing wastewater due to being extensively used in textile, printing, paper, and other industries [6], [7]. Dyes can be classified into natural and synthetic dyes. Synthetic dyes are produced from organic compounds, and they are widely used in different applications because they are easy and involve a wide range of colors with a developed formula [8], [9]. Moreover, dyes are classified based on the charge of the dye's species upon dissociation in

aqueous solutions into cationic dyes like basic dyes, anionic dyes such as acid and reactive dyes, and non-ionic dyes like dispersed dyes [10]. In addition, dyes can be categorized as soluble dyes like acidic, basic, and reactive dyes and insoluble dyes such as dispersed dyes [11].

Dye-containing wastewater is a significant type of industrial effluent that damages humans, animals, and the environment because it is undegradable and toxic [12], [13]. Dyes residue in the industrial effluents can be treated using physical, chemical, and biological techniques. These techniques include membrane filtration, adsorption [14], coagulation [15], photocatalytic [16], coagulation combined with advanced oxidation processes [17], and biosorption by algae [7]. All treatment techniques have positive and negative impacts related to the operating cost, ecosystem effect, and feasibility [18]. Purifying dyes-containing wastewater using the membrane technique has attracted more interest because it provides many benefits such as the absence of chemical materials, less energy consumption, continuous filtration mode, ease of use, small size equipment, and high separation efficiency [19], [20]. The membrane is a porous partition that allows the passage of some small particles and ions and retains others based on the pore size [21].

Based on the constituent material, membranes can be organic (polymeric) and inorganic (ceramic) membranes [20]. Polymeric membranes are considered a practical option for membranes because of their porous structure and low cost [22], [23]. Polyvinylidene fluoride (PVDF), polyacrylonitrile (PAN), polyethersulfone (PES), polyphenylsulfone (PPSU), etc. are examples of polymeric materials which are used in the membrane's fabrication [24]. Hydrophilicity, size of pores, pore size distribution, roughness, and surface charge are the parameters, which govern the permeability and selectivity of membranes [3]. The incorporation of nanomaterials into the membrane matrix represents an advanced step in improving the membrane's structure and performance and such membranes are defined as mixed matrix membranes (MMMs) [25]. The MMMs have gained increased attention because their enhanced performance contributes to reducing membrane fouling [26]. Zinc oxide, titanium oxide, silica, alumina, carbon nanotubes, etc. are examples of nanoparticles that are incorporated into the membrane casting solution [4].

Also, adding water-soluble polymers as pore forming during the demixing process is used to improve the membrane performance. Common examples of these polymers are polyethylene glycol (PEG) and polyvinylpyrrolidone (PVP) [4]. The morphological structure and performance of the membranes depend on the interaction between the polymer and additives which contributes to increasing the filtration area and improving separation efficiency [27]. Phase inversion, electrospinning, and stretching are examples of techniques used to prepare MMMs [28]. Choosing the appropriate preparation method is based on the nature of a chosen polymer and the final required structure of the membrane [29]. Phase inversion is the most common method used to fabricate MMMs because it is low cost, timesaver, easy to use, and flexible [29].

Based on the pressure difference, membrane filtration is classified into microfiltration (MF), ultrafiltration (UF), nanofiltration (NF), and reverse osmosis (RO) [30]. NF technology is widely used in water treatment because it removes the dissolved molecules effectively, depending on the pore's diameter and the repulsion between the membrane surface and pollutants [31], [32]. NF technology has a significant and essential role in the desalination and water purification from organic dyes [33]. Recently, the removal of organic compounds, dissolved molecules, and microorganisms using UF technology has gained a lot of attention because it is easy to use, clean, safe, more economical, and highly efficient [34]. NF membranes are the most effective in dye-containing wastewater treatment, but they require high operating conditions. Therefore, the trend of developing UF membranes can contribute to removing a wide range of contaminants e.g. organic dyes at low pressure conditions and low cost. Applying MMM in the UF applications to treat water pollution by dyes has experienced various nano additives. Tin oxide, likewise titanium oxide and zinc oxide, has been examined in developing the structure properties of UF membranes used in applications involving photocatalytic oxidation of organic pollutants [12]. Tin oxide attracts a lot of attention as a photoactive material and is widely used in photocatalytic processes because it has high oxidation ability, low cost, and high chemical stability [6]. However, using tin oxide in developing the filtration performance of membranes is very rare [35].

The objective of this work is to develop the PVDF membrane's performance using organic and inorganic additives for organic dye removal at UF conditions. Flat sheet PVDF membranes of 18 wt% were prepared via phase inversion and developed by

blending with PEG of 6 wt% as a pore former. The PVDF/PEG membranes were developed using tin oxide nanoparticles with different contents of 0.3, 0.6, and 0.9 wt%. The prepared membranes were characterized via field emission scanning electron microscope (FESEM), atomic force microscopy (AFM), water contact angle (CA), Fourier-transform infrared spectroscopy (FTIR), surface charge, porosity, mean pore size, tensile strength, and elongation at break. The performance was tested regarding PWF, permeate flux, and R% of the RhB dye as a model pollutant of cationic dyes. The influence of initial dye concentration and the pH of the feed solution was studied using the membrane which gave the highest performance. Also, different types of dyes were studied to calculate the molecular weight cutoff.

2 Experimental Work

2.1 *Materials*

The PVDF polymer ($(C_2H_2F_2)_n$, white powder, MW~534000 g/mol) was provided by NANOCHEMAZONE (Canada). PEG polymer ($H(OCH_2CH_2)_nOH$, MW_{av} 400 Da) was supplied from HiMedia (India) and used as an organic additive. Tin oxide nanoparticles (SnO_2 NPs, white nanopowder, pore size: 50–70 nm, and purity: 99.9%) were received from SkySpring Nanomaterials (USA). The solvent was N, N-dimethyl formamide (DMF) provided by Sigma-Aldrich (Germany). Distilled water was used as a non-solvent in the membrane's fabrication and polluted solutions preparation. The pollutants were represented by acid orange 10 (AO10, MW = 452.36 g/mol) supplied by the HiMedia (India); RhB (MW = 479.02 g/mol) purchased from Central Drug House (India); and congo red (CR, MW = 696.66 g/mol) provided by Nanjing Duly Biotech Co. (China).

2.2 *Membrane preparation*

The preparation of flat sheet membranes was achieved using the nonsolvent-induced phase separation (NIPS) technique. According to the findings of a previous work conducted by Saleem and Al-Jubouri [36], the PVDF and PEG content was fixed at 18 wt% and 6 wt%, respectively. Table 1 shows the compositions of the materials used in the membrane's preparation. The preparation of a dope solution of a membrane was done as follows: the inorganic additives (SnO_2 NPs) were mixed with the solvent (DMF) and distributed by sonication for 1 h. Then, the PEG was added to the solution and stirred at 200 rpm for 1 h using a magnetic stirrer. The PVDF was dried for 2 h at 60 °C, added to the solution, and agitated for 36 h at 35 °C and 100–150 rpm by a magnetic stirrer to obtain a homogeneous solution. The degassing of the homogeneous solution was done by sonication for 2 h then drying for 3 h at 60 °C to remove the bubbles from the solution. After the degassing process, casting the homogenous solution on a clean glass plate was done using the casting machine with a thickness of 250 µm. After that, the glass plate was placed horizontally into a coagulant bath of distilled water for 24 h at room temperature. The distilled water was changed every 8 h to remove any remaining solvent from the membrane sheet. The PM-2 and PM-1 membranes were prepared in the same way mentioned above but without incorporating SnO_2 NPs and both additives, respectively.

Table 1: Compositions of the materials used in the membrane's preparation.

Membrane Code	PVDF (wt%)	PEG (wt%)	SnO_2 NPs (wt%)	DMF (wt%)
PM-1	18	0	0	82
PM-2	18	6	0	76
PM-3	18	6	0.3	75.7
PM-4	18	6	0.6	75.4
PM-5	18	6	0.9	75.1

2.3 *Membrane characterization*

The morphology of the membrane's structure including the surface and cross-section areas was scanned by the FESEM using the Inspect TM F50 model device after the membrane's samples were cut by liquid nitrogen and sprayed with a thin layer of gold. While, the AFM was used to obtain the surface topography images and roughness parameters using NaioAFM 2022, Nanosurf. The porosity (ε) of the prepared membranes was evaluated by the gravimetric formula according to Equation (1) [37]. Additionally, the mean pore size (r_m) was calculated using the Guerout-Elford- Ferry Equation according to Equation (2) [33].

$$\varepsilon\% = \left(\frac{W_w - W_d}{A \times l \times \rho}\right) \times 100\% \quad (1)$$

$$r_m = \sqrt{\frac{(2.9 - 1.75 \times \varepsilon) \times 8 \times l \times Q \times \eta}{\varepsilon \times A \times \Delta P}} \quad (2)$$

Where: W_w is the weight of the wet membrane sample (g), W_d is the weight of the dry membrane sample (g), A is the membrane sample area (cm^2), l is the membrane sample thickness (cm), ρ is the water density (g/cm^3), Q is the pure water permeate flow rate (cm^3/s), η is the viscosity of water (Pa.s), and ΔP is the operating pressure (Pa). The CA was used to measure surface hydrophilicity using the T315A picoliter dispenser. The functional groups of the prepared membranes were examined by the FTIR with a range of 400–4000 cm^{-1} using the 1800IR spectrometer instrument. The surface charge was investigated by measuring the point of zero charge (pH_{PZC}). The tensile strength and elongation at break of the fabricated membranes were measured at room temperature using materials testing machines Testometric Co., UK with a tensile rate of 5 mm/min. It is worth mentioning that all characterizations were performed after studying the membrane's performance in the dye's removal.

2.4 *Membrane performance*

2.4.1 PWF, permeate flux, and dye removal (R%)

The PWF, permeate flux, and R% were measured in a membrane cell operating with a crossflow system and an active area of 15.4 cm^2. All experiments were run in recirculation mode at transmembrane pressure (TMP) of 1 bar, room temperature, feed flow rate of 1 L/min, and 90 min. The parameters selected to be studied herein and their ranges are shown in Table 2. The system was initially run for 30 min with pure water to obtain a steady permeation. Then, the PWF was measured using Equation (3). After measuring the PWF, the permeate flux was measured according to Equation (3) for the same period for pure water. Equation (4) was used to obtain R% simultaneously with calculating the permeate flux.

$$J = \frac{V}{A \times t} \quad (3)$$

$$R\% = \left(1 - \frac{C_P}{C_F}\right) \times 100\% \quad (4)$$

Where J is the PWF and/or permeate flux ($L/m^2.h$), V is the permeated volume (L), A is the membrane active area (m^2), and t is the permeation time (h). The C_P and C_F represent the dye's concentrations in the permeate and feed (mg/L), respectively. The concentrations of dyes in the feed and permeate solutions were calculated by a UV-9200 spectrophotometer at wavelengths 472, 494, and 546 nm for AO10, CR, and RhB, respectively.

2.4.2 Molecular weight cutoff (MWCO)

The MWCO of the membrane represents the molecular weight of dyes, which are removed by 90% using this membrane [38]. To study the MWCO of the prepared membrane, several dyes with different molecular weights were filtered at the same conditions. The results of R% were plotted versus the dye's molecular weight to evaluate the MWCO.

Table 2: The ranges of the studied parameters.

Membrane	Dye Concentration (mg/L)			pH of the Dye Solution			Dye Type		
Code	10	20	30	3	7	10	AO10	RhB	CR
PM-1	✓	-	-	-	✓	-	-	✓	-
PM-2	✓	-	-	-	✓	-	-	✓	-
PM-3	✓	-	-	✓	✓	✓	-	✓	-
	✓	✓	✓	-	✓	-	-	✓	-
	✓	-	-	-	✓	-	✓	✓	✓
PM-4	✓	-	-	-	✓	-	-	✓	-
PM-5	✓	-	-	-	✓	-	-	✓	-

2.4.3 Antifouling property and reusability of the Membranes

Studying the antifouling property gives information about the degree of enhancement of the membrane properties and the membrane fouling extent. The membrane fouling was studied by measuring the flux recovery ratio (FRR), reversible fouling (R_r), irreversible fouling (R_{ir}), and total fouling (R_t) using Equations (5)–(8), respectively [35], [39]. After calculating the J_o and J_p as mentioned above, the membranes were washed with distilled water for 10 min. Then, the PWF of the fouled membrane was evaluated using Equation (3) and recorded as J_1 for the same period.

$$FRR(\%) = \frac{J_1}{J_o} \times 100\% \quad (5)$$

$$R_r(\%) = \frac{J_1 - J_p}{J_o} \times 100\% \quad (6)$$

$$R_{ir}(\%) = \frac{J_o - J_1}{J_o} \times 100\% \quad (7)$$

$$R_t(\%) = R_r + R_{ir} = \frac{J_o - J_p}{J_o} \times 100\% \quad (8)$$

Where J_o, J_p, and J_1 are the initial PWF, permeate flux, and PWF after the membrane washing ($L/m^2 \cdot h$), respectively. Continuous reusing is an important feature of the membrane in the treatment process. The membrane performance in terms of reusability was assessed by measuring the R% using Equation (4) and antifouling analysis using Equations (5)–(8). In each cycle, the membranes were rinsed with distilled water for 10 min after running with pure water and dye solution.

3 Results and Discussion

3.1 *Characterization*

3.1.1 Morphology of the membranes

Figure 1 shows the morphology of the pure and developed membranes. Figure 1 shows all prepared membranes are asymmetric membranes formed of a dense skin layer representing the active layer and a porous layer consisting of finger-like pores and a spongy structure which represents the support layer. The PM-1 membrane texture contained fewer, shorter, and much smaller inner pores than the PM-2 membrane. This can be attributed to increasing the hydrophilicity resulting from the incorporation of PEG in the casting solution forming PM-2 membrane. The incorporation of SnO_2 NPs produced longer and denser holes than PM-2 membrane because of the hydrophilic nature of SnO_2 NPs which speeded up the demixing process between DMF and water. The texture of the PM-3 membrane contained the expanded pores, which took a horizontal direction which may contribute to enhancing the permeability. While the PM-4 membrane contained larger and denser pores than the PM-2 membrane. Unlike the PM-3 membrane, the pores of the PM-4 membrane did not take a horizontal path because high nanoparticle concentrations delayed the demixing process, which formed small cavities and improved the sieving property. This was because of the agglomeration of SnO_2 NPs on the surface during the membrane formation at high nanoparticle concentrations. These results agreed with those obtained by Hosseini *et al*. [27], Nayak *et al*. [38], and Abdullah and Al-Jubouri [40].

The top surface morphology of the pure and developed membranes is shown in Figure 1. The PM-1 membrane surface seems smooth with fine pores. The pores expanded and increased on the surface of the PM-2 membrane because of the improved hydrophilicity of the membrane resulting from adding 6 wt% of PEG. The pores on the PM-3 membrane surface became denser and wider after incorporating SnO_2 NPs. This is attributed to the high tendency of SnO_2 NPs to adsorb water which speeded up the mass transfer process during the NIPS process as shown in Figure 3(a).

3.1.2 Topography and roughness of the membranes

The AFM is used to study the surface topography and roughness parameters represented by the root mean square height (R_q), arithmetic mean height or average roughness (R_a), and maximum height (R_z) of the pure and developed membranes. Figure 2 shows the 3-D AFM images of the prepared membranes. Adding 6 wt% of PEG increased the membrane's porosity because PEG leached out during the demixing process. Similar behavior was obtained by Fadaei *et al.* [41]. Also, incorporating SnO_2 NPs created more holes on the membrane surface due to their hydrophilic nature, increasing the permeation. These results were consistent with those obtained by Nayak *et al.* [38]. Table 3 shows the porosity, mean pores size, and roughness parameters. The R_q, R_a, and R_z increased from 10.85, 8.315, and 106.3 nm for the PM-1 membrane to 75.7, 58.97, and 488.8 nm for the PM-3 membrane, respectively. The membrane surface became rougher with increasing the SnO_2 NPs concentration because they aggregated on the surface. These results agreed with those obtained by Nayak *et al.* [38] and Celic *et al.* [5].

3.1.3 Porosity and mean pore size of the membranes

The incorporation of SnO_2 NPs into the dope solution of the PM-3 membrane minimized the membrane's porosity to 58.18% and further increasing the SnO_2 NPs concentrations increased the porosity slightly to 59.14% for the PM-4 membrane. This was because the nanoparticles' agglomeration on the membrane

surface decreased the mean pore size as shown in Table 3. In the PM-4 membrane surface, the pore size grew further but not as in the PM-3 membrane because the accumulation of nanoparticles on the surface generated a resistance to water transportation. The prepared membranes can be categorized based on their mean pore size and ranges mentioned by Selatile *et al*. [42] as follows: the pure membrane was categorized as the NF membrane because it is within the NF membranes range (1–10 nm). The developed membranes were categorized as UF membranes because they are within the UF membranes range (10–100 nm).

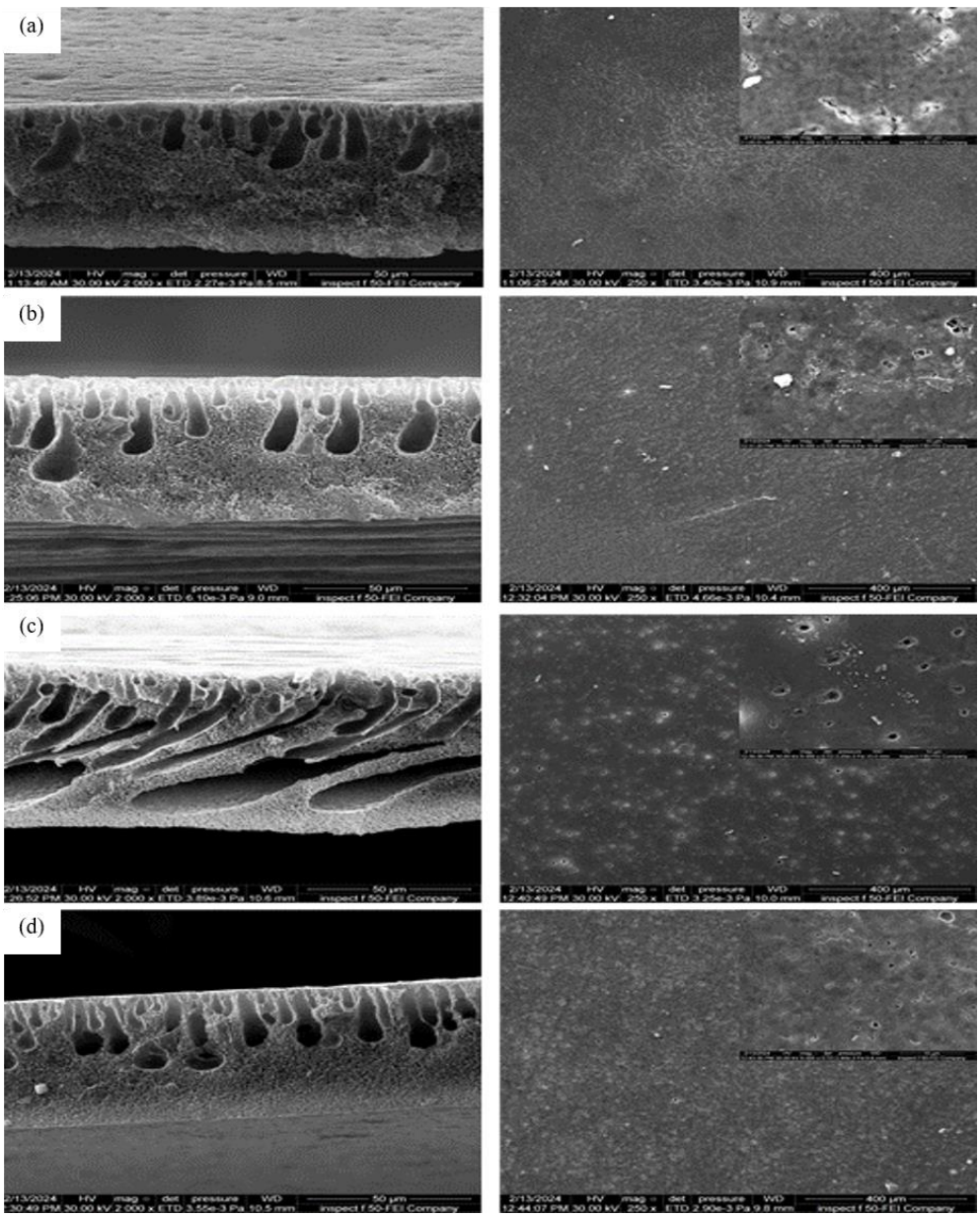

Figure 1: The FESEM images of the (a) PM-1, (b) PM-2, (c) PM-3, and (d) PM-4 membranes. The cross section on the left side with a magnification of 2000 x (50 µm) and the surface morphology on the right side with a magnification of 250 x (400 µm) and 8000 x (10 µm) for external and insets images, respectively.

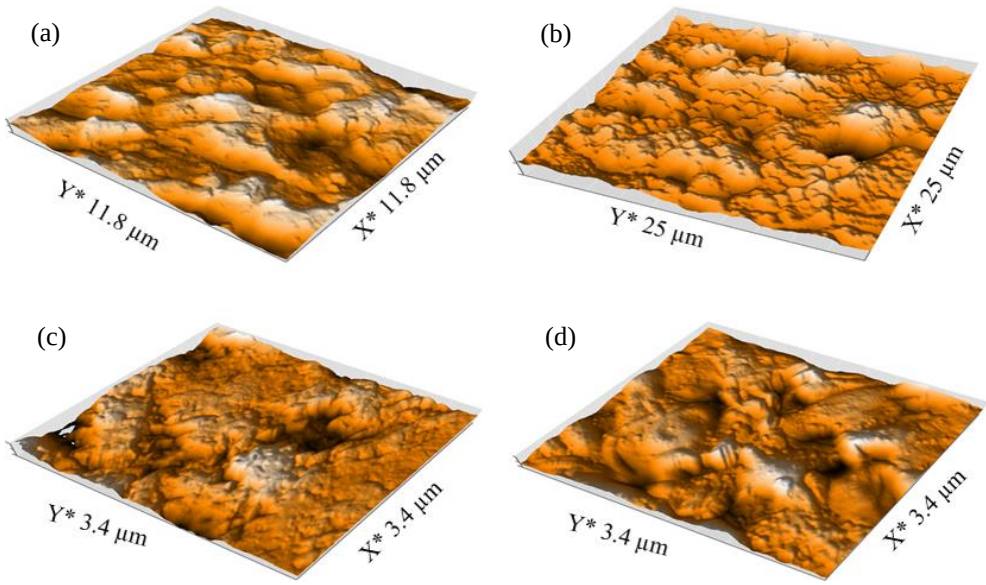

Figure 2: The 3-D images of the (a) PM-1, (b) PM-2, (c) PM-3, and (d) PM-4 membranes.

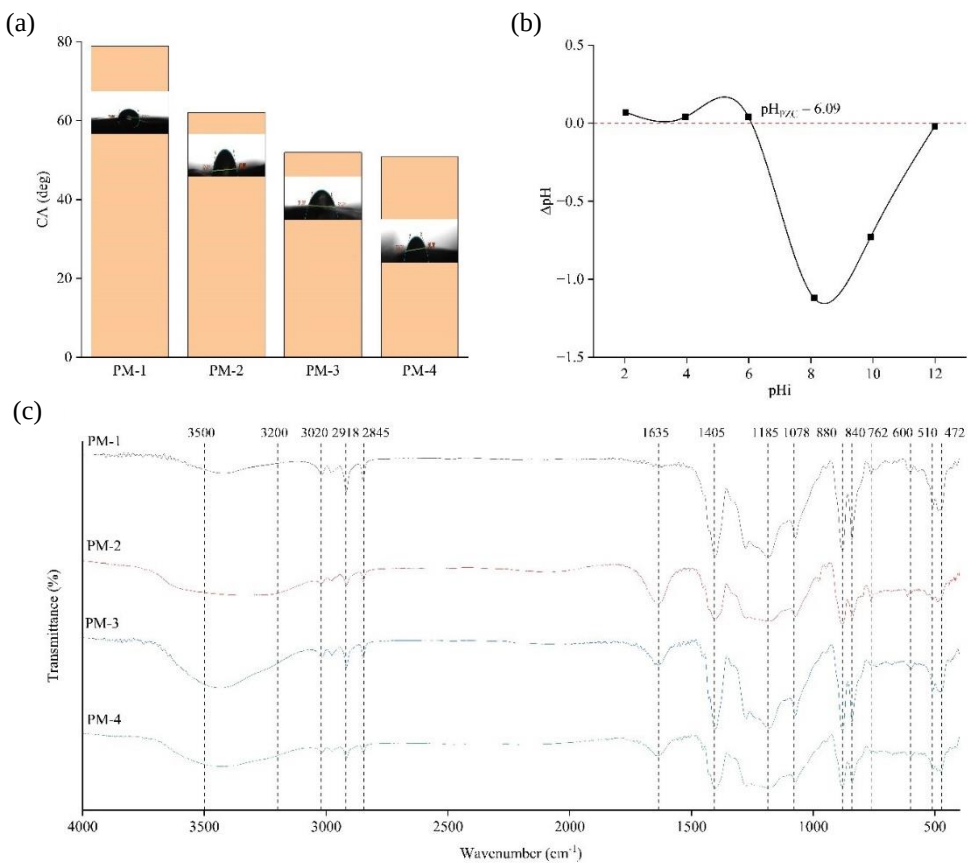

Figure 3: (a) CA of the pure and developed membranes, (b) pH_{PZC} of the PM-3 membrane, and (c) FTIR spectra of the pure and developed membranes.

Table 3: The porosity, mean pores size, and roughness parameters of the prepared membranes.

Membrane Code	Porosity (%)	Mean Pore Size (nm)	Roughness Parameters (nm)		
			R_q	R_a	R_z
PM-1	40.36	7.29	10.84	8.315	106.3
PM-2	63.07	18.23	67.55	49.69	538.8
PM-3	58.18	26.18	75.70	58.97	488.8
PM-4	59.14	24.45	99.41	77.83	656.5

3.1.4 Hydrophilicity and surface charge analysis

The effect of adding the PEG and SnO_2 NPs on the hydrophilicity of the prepared membranes can be evaluated based on the values of CA shown in Figure 3(a). The PM-1 membrane showed the highest CA value of 78.85°. Adding 6 wt% of water-soluble PEG played a significant role in enhancing the membrane hydrophilicity, as the CA decreased to 62.08° for the PM-2 membrane. Also, the incorporation of SnO_2 NPs improved the surface hydrophilicity. The CA dropped to 51.88° and 50.78° for PM-3 and PM-4 membranes, respectively. This behavior is attributed to enhancing the surface hydrophilicity of the prepared membranes by the hydrophilic SnO_2 NPs, which improve the career of the hydrophilic groups present on the membrane's surface and add some others as will be presented by the FTIR results shown in Figure 1(c). These results agreed with those obtained by Nayak *et al.* [38] and Ibrahim *et al.* [22].

The pH_{PZC} of the PM-3 membrane, which showed the highest hydrophilicity so far, was calculated as mentioned by Abbas and Al-Jubouri [43] to show the effect of the pH on the membrane surface charge and it was 6.09, as shown in Figure 1(b). Increasing the pH values led to a gradual change in the membrane surface charge from positive to negative. This result showed that in an acidic medium, high performance of the PM-3 membrane can be obtained for cationic dyes because the charges of the membrane surface and dye are positive, so repulsion is favorable, and vice versa in the basic medium.

3.1.5 FTIR analysis

Figure 3(c) shows the FTIR spectra of the pure and developed membranes. The developed membranes had a broad range of 3200–3500 cm^{-1}, which corresponds to the O-H group [44]. Also, the intensity of signals around 1635 cm^{-1} which is related to the O-H group [45], increased using PEG and SnO_2 NPs additives. The O-H group represents an indication of the membrane hydrophilicity. Therefore, increasing the range and intensity of the O-H peak refers to enhancing the surface hydrophilicity. These results agreed with those obtained by the CA testing. The signal that appeared at 1078 cm^{-1} corresponds to the stretching vibration of C-C [35]. The peaks observed at 1185, 2918, and 3020 cm^{-1} are attributed to the stretching vibration of CF_2 (a group associated with PVDF) [35], symmetric, and asymmetric stretching vibrations of CH [46], respectively. The peaks observed at 1405 and 2845 cm^{-1} are attributed to the bending vibrations of CH_2 [35] and the stretching vibration of CH_2 [6]. The peaks that appeared at 840 and 880 cm^{-1} are related to stretching vibrations of the β phase, while the α phase of PVDF is represented by signals of 762 cm^{-1} stretching vibration [35]. The peaks located at 472, 510, and 600 cm^{-1} correspond to the stretching vibration of Sn-O-Sn, which was consistent with reported by Chen *et al.* [6] and Ibrahim *et al.* [22]. The first peaks showed that SnO_2 NPs were successfully incorporated into the membrane.

3.1.6 Mechanical properties of the membranes

Measurement of the tensile strength and elongation at break of the fabricated membranes were used to study the mechanical properties of the membranes. The results shown in Figure 5(a) revealed that the highest tensile strength was 7.92 MPa for the PM-1 membrane because it has lower porosity. Adding 6 wt% PEG decreased the tensile strength to 6 MPa for the PM-2 membrane due to an increase in the membrane porosity. The incorporation of SnO_2 NPs increased tensile strength up to 6.33 MPa for the PM-3 membrane because the SnO_2 NPs act as cross-linkers to enhance the membrane's structure to endure the load stress. Increasing SnO_2 NPs concentration decreased the tensile strength to 5.83 MPa for the PM-4 membrane. The decreased tensile strength in the PM-4 membrane compared to the PM-3 membrane was because agglomeration of SnO_2 NPs in the MMM which led to the rupture of the membrane and reduced the tensile strength. An identical behaviour was obtained by Ibrahim *et al.* [22] and Hosseini *et al.* [27]. On the other hand, the elongation decreased from 12.28% for the PM-1 membrane to 6.13, 10, and 5.37% for the PM-2, PM-3, and PM-4 membranes, respectively. Excessive concentration of SnO_2 NPs in the MMM reduced the membrane toughness which resulted in decreasing the membrane elongation. Generally, similar trends were observed for the elongation at break.

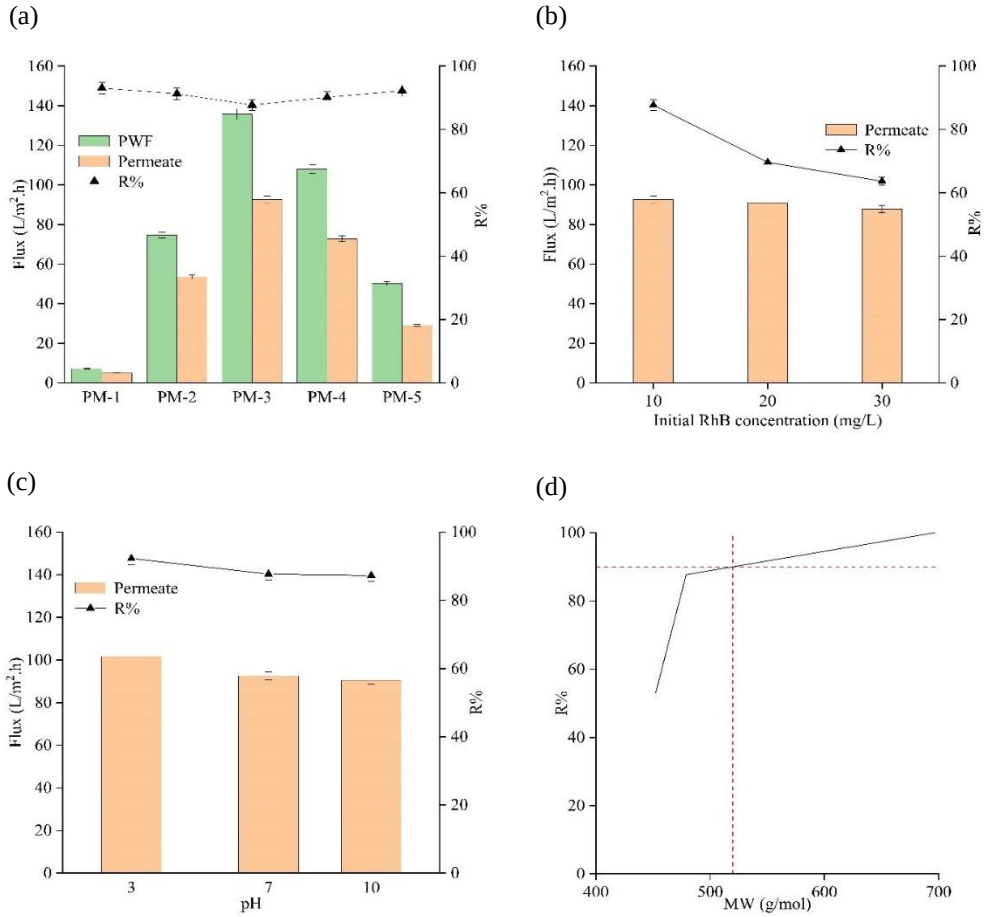

Figure 4: Effect of the (a) PEG and SnO_2 NPs on the PWF, permeate flux, and the R%, (b) initial RhB dye concentration, and (c) pH of the feed solution on the permeate flux and the R%. (d) The MWCO of the PM-3 membrane. (Filtering RhB concentration of 10 mg/L at 1 bar as TMP).

3.2 Membrane performance

3.2.1 Membrane permeation

The hydrophilicity and permeability of the pure membrane were enhanced using PEG and SnO_2 NPs. Figure 4(a) shows the effect of PEG and SnO_2 NPs on the PVDF membrane in terms of the PWF, permeate flux, and R%. Adding 6 wt% of the PEG enhanced the permeation because the pores became wider and denser as confirmed by the AFM and FESEM results. The PWF rose from 7.16 L/m^2.h for the PM-1 membrane to 74.72 L/m^2.h for the PM-2 membrane. The PWF highly improved by incorporating SnO_2 NPs up to 135.71 L/m^2.h for PM-3, then decreased to 107.92 and 50.21 L/m^2.h for PM-4 and PM-5 membranes, respectively. The R% of the RhB dye for a concentration of 10 mg/L slightly decreased from 93.08% for the PM-1 membrane to 91.26% for the PM-2 membrane and continued to decline for the PM-3 membrane to 87.71%. However, with increasing SnO_2 NPs concentration, R% rose to 90.17 and 92.23% for PM-4 and PM-5 membranes, respectively. The reason for decreasing the PWF and increasing R% with increasing SnO_2 NPs concentration was aggregation of nanoparticles on the membrane surface during the demixing process. The agglomeration of nanoparticles on the membrane surface increased the thickness of the active layer which led to decreased pore size and increased porosity, as shown in Table 3, and thus enhanced the membrane hydrophilicity as shown in Figure 3(a). These results agreed with those obtained by Hosseini *et al.* [27]. According to the obtained results, the PM-3 membrane was chosen to

conduct the other experiments because it gave an acceptable R% and higher flux than other prepared membranes.

3.2.2 Effect of the initial dye concentration

Figure 4(b) shows the effect of initial RhB dye concentration of 10, 20, and 30 mg/L on the permeate flux and R% of the PM-3 membrane. The permeate flux slightly decreased as the initial RhB dye concentration increased. The flux dropped from 92.52 to 90.91 and 87.83 L/m^2.h at 10, 20, and 30 mg/L, respectively. This was because a high dye concentration formed a cake layer on the membrane surface and reduced the flux. The R% highly decreased from 87.71 to 69.64 and 63.68 % at 10, 20, and 30 mg/L, respectively, because increasing the dye layer (concentration) on the membrane surface caused concentration polarization, which resulted in dye's molecules transportation from the membrane to the permeate side and reducing the membrane performance in the retention of dye.

3.2.3 Effect of the pH of the feed solution

The membrane surface charge should be determined because it is a function of the solution pH, and it is important to understand its behavior in the separation process. The pH_{PZC} of the PM-3 membrane was 6.09 as shown in Figure 3(b). Figure 3(b) shows that the membrane surface charge was positive at a pH lower than the pH_{PZC} and negative at a pH higher than the pH_{PZC}. Accordingly, the effect of the pH of the feed solution on the permeate flux and R% of the PM-3 membrane was studied at three pH values of 3, 7, and 10 and the results are shown in Figure 4(c). The results showed decreasing the permeate flux and R% as the pH of the feed solution increased. The reason for this behavior is that at an acidic medium (i.e. at pH = 3), both the membrane surface and pollutant carry a positive charge. Therefore, repulsion occurs between similar charges causing an increase in the permeate flux and R%. When the feed solution was basic (i.e. at pH = 10), attraction occurred between the membrane surface which has a negative charge and the pollutant carrying a positive charge. This attraction resulted in a decrease in the permeate flux and R% because accumulation of the dye molecules on the membrane surface.

3.2.4 Effect of the dye molecular weight

To study the MWCO of the PM-3 membrane, two types of dyes with different molecular weights were filtered at the same conditions. The selected dyes were RhB as a cationic dye, AO10 and CR as anionic dyes with a concentration of 10 mg/L. The R% were 53.07, 87.71, and 100% for AO10, RhB, and CR, respectively. Based on these results, the MWCO of the PM-3 membrane was 520 Da as shown in Figure 4(d). This means that the PM-3 membrane can remove 90% of the dyes with molecular weight above 520 Da. Table 4 shows a detailed comparison between the performance of the PM-3 membrane and other developed membranes prepared in previous studies based on the most important factors and items. The PVDF/PEG-SnO_2 (0.3 wt%) membrane achieved acceptable permeation and dye removal performance at low pressure conditions.

Table 4: Comparison of the PM-3 membrane performance with previous works.

Base Polymer	Additives	Dye	Concentration (mg/L)	Pressure (bar)	Permeate Flux (L/m^2.h)	Filtration Efficiency (%)	MWCO (Da)	Ref.
PVDF (12 wt%)	PEG (4 wt%)	Reactive red 141	15	6	N/A	77	980	[47]
PPSU (16 wt%)	PVP (4 wt%) SnO_2 (0.4 wt%)	Reactive black-5 Reactive orange-16	50	2	109.77 169.16	73 94	1800	[38]
Acrylic fiber waste (AF) (20 wt%)	PVP (5 wt%)	Methylene blue CR Crystal violet	20	3	300 320 N/A	90 100 100	320	[48]
PVDF (18 wt%)	PEG (6 wt %)	AO10 RhB CR	10	1	57.06 53.56 51.31	57.83 91.26 100.0	478	[36]
PVDF (18 wt%)	PEG (6 wt %) SnO_2 NPs (0.3 wt%)	AO10 RhB CR	10	1	95.45 92.52 87.14	53.07 87.71 100.0	520	Current study

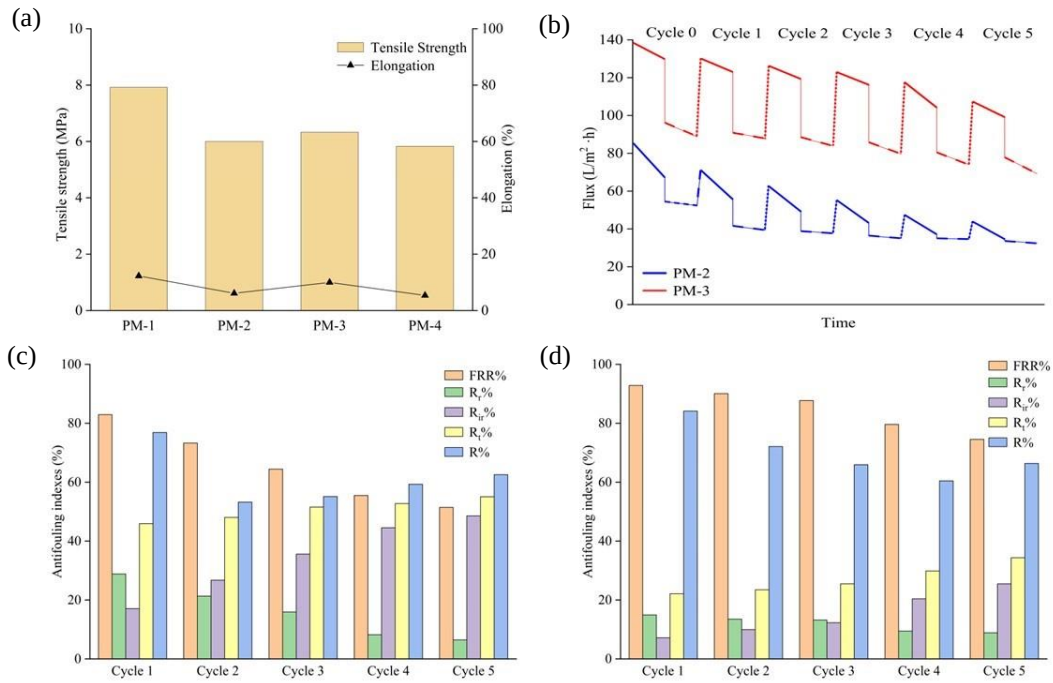

Figure 5: (a) Mechanical properties of the prepared membranes, (b) effect of washing on the performance of the reusable PM-2 and PM-3 membranes (Solid line: pure water; dash line: dye solution; dot line: washing), (c) antifouling analysis of the cycles of the PM-2 membrane, and (d) antifouling analysis of the cycles of the PM-3 membrane. (Filtering RhB concentration of 10 mg/L at 1 bar as TMP).

3.2.5 Antifouling property and reusability of the Membranes

The effect of washing on the flux of the usable PM-2 and PM-3 membranes is shown in Figure 5(b). The results showed that the permeation of the membranes continuously decreased because of the increased concentration polarization, which caused increasing fouling. The efficacy of the cleaned membranes in the successive removal cycles revealed the membrane's ability to retain the dye's molecules. The PM-2 membrane offered a high ability for adsorbing the dye molecules, which led to an obvious decrease in the flux even after washing because the adsorbed and accumulated molecules on the surface cannot be completely removed by washing. The performance of the PM-3 membrane after each washing was better because it has lower CA as shown in Figure 3(a), which resulted in a more hydrophilic surface and higher resistance to dye molecules adsorption than the PM-2 membrane. This expression was consistent with that reported by Sadek and Al-Jubouri [1], who mentioned that hydrophilic membranes offer high resistance to the adsorption of foulants.

Figure 5(c) and (d) show the antifouling analysis in terms of the FRR%, R_r%, R_{ir}%, R_t%, and R% obtained for each cycle run using the PM-2 and PM-3 membranes, respectively. The FRR% was evaluated to show the extent molecules adhering to the membrane's surface. The FRR% values of the PM-2 and PM-3 membranes were 82.94% and 92.82% then decreased to 51.43% and 74.52% after five times of reusing, respectively. Adsorbed molecules on the surface of the PM-2 membrane were incompletely removed by washing after cycle 2 because increasing the adhesion ability of dye molecules on the membrane surface resulted in decreased permeation and improved the sieving properties. While in the PM-3 membrane, the dye molecules were distinguishably removed as confirmed by the values of R_r% obtained until cycle 4 because the PM-3 membrane was very hydrophilic and offered higher resistance to the dye molecule's adhesion. The reduction in R% value was marginally stable for both PM-2 and PM-3 membranes because of the continuous accumulation of dye molecules, which was confirmed by increasing R_{ir}% values. The formation of a cake layer on the surface restricted the permeability and enhanced the R%. An identical behavior was obtained by Aljanabi *et al*. [4].

4 Conclusions

The PVDF flat sheet membranes were successfully developed by incorporating the PEG and SnO_2 NPs using the NIPS process to be used in the organic dye removal at UF conditions. Incorporating PEG and SnO_2 NPs changed the membrane morphology and topography and enhanced the hydrophilicity and permeation. The CA decreased from 78.85° to 62.08° and 51.88°, the PWF rose from 7.16 to 74.72 then up to 135.71 $L/m^2.h$, and the R% of 10 mg/L RhB concentration slightly decreased from 93.08% to 91.26 and 87.71% for PVDF, PVDF/PEG, and PVDF/PEG-SnO_2 membranes, respectively. Increasing SnO_2 NPs concentration above 0.3% caused agglomeration of nanoparticles on the membrane surface and thus increased the thickness of the active layer, which decreased the permeability and increased the R%. Increasing the concentration polarization on the membrane surface as the initial dye concentration increased caused a slight decrease in the permeate flux and an obvious decrease in the R%. High performance was obtained when the charges of the membrane surface and dye were similar. The retention of the PVDF/PEG-SnO_2 NPs membranes was lower than of the PVDF/PEG membrane because it has higher hydrophilicity through providing a protective hydration layer, which resulted in high surface resistance to dye molecules adsorption. The membrane containing 0.3 wt% SnO_2 NPs can be used to remove 90% of both cationic and anionic dyes having a molecular weight above 520 Da at UF conditions with high permeation. Accordingly, the PVDF/PEG-SnO_2 NPs membranes can be potentially recommended for treating industrial wastewater containing various dyes or other pollutants i.e. divalent ions and salts. Also, the performance of these membranes can be tested in the photocatalysis process to remove persistent pollutants.

Author Contributions

A.G.S.: investigation, methodology, data curation, writing an original draft, research design, data analysis; S.M.A.: investigation, methodology, reviewing and editing, research design, data analysis, project administration. Both authors have read and agreed to the published version of the manuscript.

Conflicts of Interest

The authors declare no conflict of interest.

References

[1] S. A. Sadek and S. M. Al-Jubouri, "Structure and performance of polyvinylchloride microfiltration membranes improved by green silicon oxide nanoparticles for oil-in-water emulsion separation," *Materials Today Sustainability*, vol. 24, 2023, doi: 10.1016/j.mtsust.2023.100600.

[2] S. Yadav and S. Kamsonlian, "Progress on the development of techniques to remove contaminants from wastewater a review," *Applied Science and Engineering Progress*, vol. 16, no. 3, 2023, Art. no. 6729, doi: 10.14416/j.asep.2023.02.001.

[3] A. M. Ali, K. T. Rashid, A. A. Yahya, H. S. Majdi, I. K. Salih, K. Yusoh, Q. F. Alsalhy, A. A. Abdul Razak, and A. Figoli, "Fabrication of gum arabic-graphene (Gga) modified polyphenylsulfone (ppsu) mixed matrix membranes: A systematic evaluation study for ultrafiltration (uf) applications," *Membranes (Basel)*, vol. 11, no. 7, 2021, doi: 10.3390/membranes11070542.

[4] A. A. A. Aljanabi, N. E. Mousa, M. M. Aljumaily, H. S. Majdi, A. A. Yahya, M. N. AL-Baiati, N. Hashim, K. T. Rashid, S. Al-Saadi, and Q. F. Alsalhy, "Modification of polyethersulfone ultrafiltration membrane using poly(terephthalic acid-co-glycerol-g-maleic anhydride) as novel pore former," *Polymers (Basel)*, vol. 14, no. 16, 2022, doi: 10.3390/polym14163408.

[5] N. Ćelić, N. Banić, I. Jagodić, R. Yatskiv, J. Vaniš, G. Strbac, and S. Lukić-Petrović, "Eco-Friendly Photoactive Foils Based on ZnO/SnO_2-PMMA Nanocomposites with High Reuse Potential," *ACS Applied Polymer Materials*, vol. 5, no. 5, pp. 3792–3800, 2023, doi: 10.1021/acsapm.3c00396.

[6] Y. Chen, Y. Jiang, B. Chen, F. Ye, H. Duan, and H. Cui, "Facile fabrication of N-doped carbon quantum dots modified SnO_2 composites for improved visible light photocatalytic activity," *Vacuum*, vol. 191, 2021, doi: 10.1016/j.vacuum.2021.110371.

[7] A. A. Najim and A. A. Mohammed, "Biosorption of Methylene Blue from Aqueous Solution Using Mixed Algae," *Iraqi Journal of Chemical and Petroleum Engineering*, vol. 19, no. 4, pp. 1–11, 2018, doi: 10.31699/ijcpe.2018.4.1.

[8] O. I. Lipskikh, E. I. Korotkova, Y. P. Khristunova, J. Barek, and B. Kratochvil, "Sensors for voltammetric determination of food azo dyes - A

critical review," *Electrochimica Acta*, vol. 260, pp. 974–985, 2018. doi: 10.1016/j.electacta.2017.12.027.

[9] S. Yadav, K. S. Tiwari, C. Gupta, M. K. Tiwari, A. Khan, and S. P. Sonkar, "A brief review on natural dyes, pigments: Recent advances and future perspectives," *Results in Chemistry*, vol. 5, 2023. doi: 10.1016/j.rechem.2022.100733.

[10] M. T. Yagub, T. K. Sen, S. Afroze, and H. M. Ang, "Dye and its removal from aqueous solution by adsorption: A review," *Advances in Colloid and Interface Science*, vol. 209, pp. 172–184, 2014, doi: 10.1016/j.cis.2014.04.002.

[11] S. M. Al-Jubouri, H. A. Al-Jendeel, S. A. Rashid, and S. Al-Batty, "Green synthesis of porous carbon cross-linked Y zeolite nanocrystals material and its performance for adsorptive removal of a methyl violet dye from water," *Microporous and Mesoporous Materials*, vol. 356, 2023, doi: 10.1016/j.micromeso.2023.112587.

[12] A. Sadeghzadeh-Attar, "Binary Zn-doped SnO_2/Al_2O_3 nanotube composites for visible-light-driven photocatalytic degradation of basic blue 41," *ACS Applied Nano Materials*, vol. 3, no. 10, pp. 9931–9942, 2020, doi: 10.1021/acsanm.0c01939.

[13] S. H. Ahmed, E. A. A. Rasheed, L. A. A. Rasheed, and F. R. Abdulrahim, "Decolorization of cationic dye from aqueous solution by multiwalled carbon nanotubes," *Journal of Ecological Engineering*, vol. 25, no. 2, pp. 72–84, 2024, doi: 10.12911/22998993/176210.

[14] A. B. D. Nandiyanto, S. N. Hofifah, H. T. Inayah, I. F. Yani, S. R. Putri, S. S. Apriliani, S. Anggraeni, D. Usdiyana, and A. Rahmat, "Adsorption isotherm of carbon microparticles prepared from pumpkin (*cucurbita maxima*) seeds for dye removal," *Iraqi Journal of Science*, vol. 62, no. 5, pp. 1404–1414, 2021, doi: 10.24996/ijs.2021.62.5.2.

[15] A. Al-Hemiri, H. Al-Anbari, and I. K. Shakir, "Dye removal from wastewater using iron salts," *Iraqi Journal of Chemical and Petroleum Engineering*, vol. 9, no. 3, pp. 17–24, 2008.

[16] N. A. Mohammed, A. I. Alwared, and M. S. Salman, "Photocatalytic degradation of reactive yellow dye in wastewater using H_2O_2/TiO_2/UV technique," *Iraqi Journal of Chemical and Petroleum Engineering*, vol. 21, no. 1, pp. 15–21, 2020, doi: 10.31699/ijcpe.2020.1.3.

[17] P. Kiattisaksiri, N. Petmark, and T. Ratpukdi, "Combination of coagulation and VUV+H_2O_2 for the treatment of color and organic matter in treated effluent wastewater from a sugar factory," *Applied Science and Engineering Progress*, vol. 16, no. 4, 2023, Art. no. 6192, doi: 10.14416/j.asep.2022.08.002.

[18] S. Samsami, M. Mohamadi, M. H. Sarrafzadeh, E. R. Rene, and M. Firoozbahr, "Recent advances in the treatment of dye-containing wastewater from textile industries: Overview and perspectives," *Process Safety and Environmental Protection*, vol. 143, pp. 138–163, 2020, doi: 10.1016/j.psep.2020.05.034.

[19] H. N. Alfalahy and S. M. Al-Jubouri, "Preparation and application of polyethersulfone ultrafiltration membranincorporating NaX zeolite for lead ions removal from aqueous solutions," *Desalination Water Treat*, vol. 248, pp. 149–162, 2022, doi: 10.5004/dwt.2022.28072.

[20] R. Suresh, S. Rajendran, L. Gnanasekaran, P. L. Show, W. H. Chen, and M. Soto-Moscoso, "Modified poly(vinylidene fluoride) nanomembranes for dye removal from water – A review," *Chemosphere*, vol. 322, 2023, doi: 10.1016/j.chemosphere.2023.138152.

[21] V. Vatanpour, S. S. . Khadem, A. Dehqan, M. A. Al-Naqshabandi, M. R. Ganjali, S. S. Hassani, M. R. Rashid, M. R. Saeb, and N. Dizge, "Efficient removal of dyes and proteins by nitrogen-doped porous graphene blended polyethersulfone nanocomposite membranes," *Chemosphere*, vol. 263, 2021, doi: 10.1016/j.chemosphere.2020.127892.

[22] Y. Ibrahim, V. Naddeo, F. Banat, and S. W. Hasan, "Preparation of novel polyvinylidene fluoride (PVDF)-Tin(IV) oxide (SnO_2) ion exchange mixed matrix membranes for the removal of heavy metals from aqueous solutions," *Separation and Purification Technology*, vol. 250, 2020, doi: 10.1016/j.seppur.2020.117250.

[23] N. H. M. Safari, S. Rozali, A. R. Hassan, and R. Osman, "Inducing the skinned-oriented asymmetrical nanofiltration membranes via controlled evaporation times in dry wet phase inversion process," *Applied Science and Engineering Progress*, vol. 16, no. 2, 2023, Art. no. 6015, doi: 10.14416/j.asep.2022.05.007.

[24] R. J. Kadhim, F. H. Al-Ani, M. Al-Shaeli, Q. F. Alsalhy, and A. Figoli, "Removal of dyes using graphene oxide (Go) mixed matrix membranes," *Membranes (Basel)*, vol. 10, no. 12, pp. 1–24, 2020, doi: 10.3390/membranes10120366.

[25] S. M. Al-Jubouri, S. Al-Batty, R. K. S. Al-Hamd, R. Sims, M. W. Hakami, and S. K. Manirul Haque, "Sustainable environment through using porous materials: A review on wastewater treatment," *Asia-Pacific Journal of Chemical Engineering*, 2023. doi: 10.1002/apj.2941.

[26] R. M. Al-Maliki, Q. F. Alsalh, S. Al-Jubouri, A. A. AbdulRazak, M. A. Shehab, Z. Németh, K. Hernadi, and H S. Majdi, "Enhanced Antifouling in Flat-Sheet Polyphenylsulfone Membranes Incorporating Graphene Oxide–Tungsten oxide for ultrafiltration applications," *Membranes (Basel)*, vol. 13, no. 3, 2023, doi: 10.3390/membranes13030269.

[27] S. M. Hosseini, F. Karami, S. K. Farahani, S. Bandehali, J. Shen, E. Bagheripour, and A. Seidypoor "Tailoring the separation performance and antifouling property of polyethersulfone based NF membrane by incorporating hydrophilic CuO nanoparticles," *Korean Journal of Chemical Engineering*, vol. 37, no. 5, pp. 866–874, 2020, doi: 10.1007/s11814-020-0497-2.

[28] M. R. Esfahani, S. A. Aktij, Z. Dabaghian, M. D. Firouzjaei, A. Rahimpour, J. Eke, I. C. Escobar, M. Abolhassani, L. F. Greenlee, A. R. Esfahani, A. Sadmani, and N. Koutahzadeh, "Nanocomposite membranes for water separation and purification: Fabrication, modification, and applications," *Separation and Purification Technology*, vol. 213, pp. 465–499, 2019. doi: 10.1016/j.seppur.2018.12.050.

[29] A. Nasir, F. Masood, T. Yasin, and A. Hameed, "Progress in polymeric nanocomposite membranes for wastewater treatment: Preparation, properties and applications," *Journal of Industrial and Engineering Chemistry*, vol. 79, pp. 29–40, 2019, doi: 10.1016/j.jiec.2019.06.052.

[30] N. Mustafa and H. Al -Nakib, "Reverse Osmosis Polyamide Membrane for the Removal of Blue and Yellow Dye from Waste Water," *Iraqi Journal of Chemical and Petroleum Engineering*, vol. 14, no. 2, pp. 49–55, 2013.

[31] L. Liu, X. Chen, S. Feng, Y. Wan, and J. Luo, "Enhancing the antifouling ability of a polyamide nanofiltration membrane by narrowing the pore size distribution via one-step multiple interfacial polymerization," *ACS Applied Materials & Interfaces*, vol. 14, no. 31, pp. 36132–36142, 2022, doi: 10.1021/acsami.2c09408.

[32] S. Hadi, A. A. Mohammed, S. M. Al-Jubouri, M. F. Abd, H. S. Majdi, Q. F. Alsalhy, K. T. Rashid, S. S. Ibrahim, I. K. Salih, and A. Figoli, "Experimental and theoretical analysis of lead Pb^{2+} and Cd^{2+} retention from a single salt using a hollow fiber PES membrane," *Membranes (Basel)*, vol. 10, no. 7, pp. 1–25, 2020, doi: 10.3390/membranes10070136.

[33] G. Gnanasekaran, M.S.P. Sudhakaran, D. Kulmatova, J. Han, G. Arthanareeswaran, E. Jwa, and Y. S. Mok, "Efficient removal of anionic, cationic textile dyes and salt mixture using a novel CS/MIL-100 (Fe) based nanofiltration membrane," *Chemosphere*, vol. 284, 2021, doi: 10.1016/j.chemosphere.2021.131244.

[34] R. M. Al-Maliki, Q. F. Alsalh, S. Al-Jubouri, I. K. Salih, A. A. AbdulRazak, M. A. Shehab, Z. Németh, and K. Hernadi, "Classification of nanomaterials and the effect of Graphene Oxide (GO) and recently developed nanoparticles on the ultrafiltration membrane and their applications: A review," *Membranes*, vol. 12, 2022, Art. no. 1043, doi: 10.13140/RG.2.2.14364.16001.

[35] Z. Chen, G. Chen, H. Xie, Z. Xu, Y. Li, J. Wan, L. Liu, and H. Mao, "Photocatalytic antifouling properties of novel PVDF membranes improved by incorporation of SnO_2-GO nanocomposite for water treatment," *Separation and Purification Technology*, vol. 259, 2021, doi: 10.1016/j.seppur.2020.118184.

[36] A. G. Saleem and S. M. Al-Jubouri, "Separation performance of cationic and anionic dyes from water using polyvinylidene fluoride-based ultrafiltration membrane incorporating polyethylene glycol," *Desalination Water Treat*, 2024, Art. no. 100546, doi: 10.1016/j.dwt.2024.100546.

[37] K. Umam, F. Sagita, E. Pramono, M. Ledyastuti, G. T. M. Kadja, and C. L. Radiman, "Polyvinylidenefluoride (PVDF)/ surface functionalized- mordenite mixed matrix membrane for congo red dyes removal: Effect of types of organosilane," *JCIS Open*, vol. 11, 2023, doi: 10.1016/j.jciso.2023.100093.

[38] M. C. Nayak, A. M. Isloor, Inamuddin, B. Prabhu, N. I. Norafiqah, and A. M. Asiri, "Novel polyphenylsulfone (PPSU)/nano tin oxide (SnO_2) mixed matrix ultrafiltration hollow fiber membranes: Fabrication, characterization and toxic dyes removal from aqueous solutions," *Reactive and Functional Polymers*, vol. 139, pp. 170–180, 2019, doi: 10.1016/j.reactfunctpolym.2019.02.015.

[39] S. Liu, X. Fang, M. Lou, Y. Qi, R. Li, G. Chen, Y. Li, Y. Liu, and F. Li, "Construction of loose positively charged nf membrane by layer-by-layer grafting of polyphenol and polyethyleneimine on the pes/fe substrate for dye/salt separation," *Membranes (Basel)*, vol. 11, no. 9, 2021, doi: 10.3390/membranes11090699.

[40] M. Abdullah and S. Al-Jubouri, "Implementation of hierarchically porous zeolite-polymer membrane for Chromium ions removal," in *IOP Conference Series: Earth and Environmental Science*, 2021. doi: 10.1088/1755-1315/779/1/012099.

[41] A. Fadaei, A. Salimi, and M. Mirzataheri, "Structural elucidation of morphology and performance of the PVDF/PEG membrane," *Journal of Polymer Research*, vol. 21, no. 9, 2014, doi: 10.1007/s10965-014-0545-x.

[42] M. K. Selatile, S. S. Ray, V. Ojijo, and R. Sadiku, "Recent developments in polymeric electrospun nanofibrous membranes for seawater desalination," *RSC Advances*, vol. 8, no. 66. Royal Society of Chemistry, pp. 37915–37938, 2018. doi: 10.1039/C8RA07489E.

[43] S. M. Abbas and S. M. Al-Jubouri, "High performance and antifouling zeolite@ polyethersulfone/cellulose acetate asymmetric membrane for efficient separation of oily wastewater," *Journal of Environmental Chemical Engineering*, vol. 12, no. 3, 2024, doi: 10.1016/j.jece.2024.112775.

[44] S. J. Jie, O. B. Seng, L. L. H. Ting, and S. J. Yao, "Development of antifouling poly(vinylidene fluoride) ultrafiltration membrane with the addition of polyethylene glycol as additive," in *IOP Conference Series: Earth and Environmental Science*, Institute of Physics Publishing, 2020, doi: 10.1088/1755-1315/463/1/012178.

[45] J. Zhu, S. Zhou, M. Li, A. Xue, Y. Zhao, W. Peng, and W. Xing, "PVDF mixed matrix ultrafiltration membrane incorporated with deformed rebar-like Fe_3O_4–palygorskite nanocomposites to enhance strength and antifouling properties," *Journal of Membrane Science*, vol. 612, 2020, doi: 10.1016/j.memsci.2020.118467.

[46] M. Sri Abirami Saraswathi, R. Kausalya, N. J. Kaleekkal, D. Rana, and A. Nagendran, "BSA and humic acid separation from aqueous stream using polydopamine coated PVDF ultrafiltration membranes," *Journal of Environmental Chemical Engineering*, vol. 5, no. 3, pp. 2937–2943, 2017, doi: 10.1016/j.jece.2017.05.051.

[47] N. Nikooe and E. Saljoughi, "Preparation and characterization of novel PVDF nanofiltration membranes with hydrophilic property for filtration of dye aqueous solution," *Applied Surface Science*, vol. 413, pp. 41–49, 2017, doi: 10.1016/j.apsusc.2017.04.029.

[48] A. E. Abdelhamid, A. E. Elsayed, M. Naguib, and E. A. Ali, "Effective dye removal by acrylic-based membrane constructed from textile fibers waste," *Fibers and Polymers*, 2023, doi: 10.1007/s12221-023-00247-z.